*This document is not available in an electronic format. A copy of this document is available at the Carlsbad, New Mexico Public Library or at one of the other nine EPA Docket libraries maintained for such purposes.*

SAND78-0566
copy 1.

SAND-78-0566
Unlimited Release

# NUCLEAR WASTE CANISTER THERMALLY INDUCED MOTION

P. R. Dawson and J. R. Tillerson


2900 Q(7-73)

Record Copy


2900 Q(7-73)

Record Copy

Issued by Sandia Laboratories, operated for the United States Department of Energy by Sandia Corporation.



Printed in the United States of America
Available from
National Technical Information Service
U. S. Department of Commerce
5285 Port Royal Road
Springfield, VA 22161
Price: Printed Copy $4.00; Microfiche $4.50

SAND-78-0566
Unlimited Release
Printed June 1978

# NUCLEAR WASTE CANISTER THERMALLY INDUCED MOTION

P. R. Dawson and J. R. Tillerson
Computational Physics & Mechanics Division I - 5162
Sandia Laboratories, Albuquerque, New Mexico 87185

## ABSTRACT

The movement of canisters containing heat producing nuclear wastes has been analyzed using a single canister model in a salt environment. Steady state and transient analyses both indicate that only minimal canister movement will result from buoyancy of heated salt.

TABLE OF CONTENTS

# I. INTRODUCTION

The movement of canisters containing heat generating nuclear wastes buried in a salt repository has been questioned. The existence of buoyant forces due to thermally produced density differences suggests the possibility of initiating convective cells in a plastic medium like salt. A proper assessment of this motion includes consideration of the temperature dependence of the effective viscosity and thermal conductivity of the salt as well as decrease in the thermal output of the heat generating wastes with time.

A thermomechanically coupled formulation for creeping viscous flow and heat transfer that includes the features mentioned earlier has been used to predict canister motion. The large deformation creeping behavior of the salt over long periods of time was represented as a viscous fluid with temperature dependent viscosity. Deformations were required to be incompressible and elastic response of the salt was assumed to be negligible in comparison to the viscous strains. The conductive-convective heat transfer equation was solved to obtain the temperature distributions within the salt-canister system. Temperature dependent thermal conductivity was included in the analyses. Coupling between the flow field and temperature distribution resulted from temperature dependent material properties, temperature dependent body forces, viscous dissipation and changes in the system geometry. The Boussinesq approximation was applied in these analyses so that only the body forces in the equilibrium equation were affected by changes in the salt density. Free expansion of the salt with temperature rises was assumed for the purpose of computing these body forces. This assumption led to the largest density differences and

therefore the greatest driving forces for upward salt flow. Separate thermoelastic computations were performed to evaluate the validity of this free expansion assumption.

An axisymmetric region 500 m in radius that extended 750 m above and below the canister elevation was analyzed. Transient creeping flow and heat transfer analyses began with an initial undeformed isothermal region and followed the movement of the canister as the salt heated and a convective cell formed. The heat source resulted from the radioactive decay of the wastes in the canister. The source diminished with time based on a thirty year half life (a realistic approximation for heat producing nuclear wastes). The temperature fields predicted in the transient analyses served as input to the thermoelastic studies. Steady-state creeping flow and heat transfer analyses were used to predict an upper bound on the magnitude of velocities. For the steady-state analyses, velocity fields and temperature distributions were computed assuming that the canister thermal output was constant (and equal to the maximum power for all times). Because the waste heat output decays with time, the actual temperatures would never reach values predicted using the constant source. Thus, velocities predicted using the steady-state temperature field grossly overestimate actual velocities.

## II. THERMOMECHANICAL SOLUTION METHODS

Computer codes based on the finite element method were utilized to predict the creeping viscous and thermoelastic expansion of the salt in the region of analysis. The creeping viscous flow computations were performed using the COUPLEFLO [1,2,3] code. The thermoelastic computations were made with the Sandia version of the BMINES [4] program.

COUPLEFLO is based on a formulation for creeping incompressible non-Newtonian fluid flow. The Euler equations resulting from the variational principle for this formulation are:

$$\frac{\partial \sigma_{ij}}{\partial x_j} + \rho g_i = 0 \tag{1}$$

$$\dot{\epsilon}_{ij} = \frac{1}{2}\left(\frac{\partial u_i}{\partial x_j} + \frac{\partial u_j}{\partial x_i}\right) \tag{2}$$

$$\dot{\epsilon}'_{ij} = \sigma_{ij}/2\mu \tag{3}$$

$$\dot{\epsilon}_{ii} = 0 \tag{4}$$

$$\rho = \rho_o(1 - \alpha\Delta T) \tag{5}$$

where $\sigma_{ij}$ and $\sigma'_{ij}$ are the stress and stress deviator tensors; $\dot{\epsilon}_{ij}$ is the strain-rate tensor; $u_i$ is the velocity vector; $g_i$ is the gravity vector; $\rho$ is the density; $\alpha$ is the volumetric expansivity; $\mu$ is the viscosity; and $\Delta T$ is the temperature rise.

Equation (1) represents a force balance on the salt. In this equation the acceleration terms have been neglected, limiting the validity

of the analyses to flows in which the inertia may be neglected in comparison to other terms in the equation. Equation (2) is a kinematic relationship between strain-rate and velocity. Equation (3) is the constitutive model used to approximate the secondary creep behavior of the salt. In the analyses presented, the viscosity is either constant or temperature dependent. Often, a Bingham viscoplastic model having a minimum yield stress before flow begins is used to model the salt response. Experiments performed at Sandia [5] indicate that the yield stress is negligible and that flow begins with very low stress values. In this case the Bingham model is equivalent to the model described by Equation (3). Equation (4) represents the incompressibility constraint placed on the allowed mode of deformations. Equation (5) indicates the relationship between salt density and changes in temperatures. Known velocities or traction vectors are applied along the boundaries.

The heat transfer formulation in COUPLEFLO is based on the conductive-convective energy equation:

$$\frac{\partial}{\partial x_i}\left(k\frac{\partial T}{\partial x_i}\right) - \rho C_p u_i \frac{\partial T}{\partial x_i} + Q = \rho C_p \frac{\partial T}{\partial \tau} \qquad (6)$$

where T is the temperature; k is the conductivity; $C_p$ is the specific heat; Q is the heat generation rate; and $\tau$ is time. The heat generation rate, Q, decays with a prescribed half life in the transient analyses. Temperature dependent conductivity has been used in the analyses as indicated in the results. Known temperatures or heat fluxes are applied along the boundaries.

The finite element equations are formulated from a variational principle for the viscous flow equations and using Galerkin's method for

the energy equation. Application of the Boussinesq approximation in the formulation specifies that changes in density should be considered only when computing the body forces and neglected elsewhere. The equations of motion (Equations (1)-(5)) are coupled to the energy equation (Equation (6)) through viscous dissipation, temperature dependent material properties, temperature dependent body forces, material convection, and changing geometry.

Transient analysis performed using COUPLEFLO begins with an undeformed isothermal salt medium and proceeds incrementally through time. First, the velocity distribution is determined from the momentum equations with material properties and body forces based on the salt at its initial temperature. The temperature distribution corresponding to the end of the first time step is then determined by solving the energy equation using a Crank-Nicholson finite difference method in the time domain. The salt geometry then moved ahead to its deformed configuration at the end of the first time step though Euler integration of the velocity field. Subsequent movement of the salt is evaluated by continuing to step the solution ahead, each time using the velocities and temperatures at the end of the prior time step as initial conditions for the new time step.

The steady-state analyses in COUPLEFLO are performed using an iterative technique that alternates between creeping viscous flow solutions and temperature solutions. First, the temperature distribution is determined assuming no motion in the salt. Next the velocity field is determined using the temperature distribution previously obtained to define material properties and body forces. Then a new temperature distribution is obtained that includes viscous dissipation and material convection computed using the velocity field. The analysis continues to alternate

back and forth between solutions until the coupled temperature distribution and velocity field do not change from one iteration to the next. At this point, the velocity field determined from the temperature distribution is consistent with the temperature distribution obtained using the material convection and viscous dissipation resulting from that velocity field.

*COUPLEFLO* uses isoparametric triangular elements with quadratic velocity approximations and linear pressure approximations. It employs a frontal solution technique with Cholesky decomposition to solve the matrix equations resulting from the finite element formulations.

The SANDIA-BMINES computer program is formulated for static, two- or three-dimensional stress analyses. The material properties package has been written especially to represent the response of geologic media. Both isotropic and anisotropic material behavior can be simulated using linear and nonlinear models. Thermoelastic stress distributions and deformations can be computed using SANDIA-BMINES. The code does not have the capabilities for heat transfer analyses, so provisions have been made for specifying the temperature field prior to the thermoelastic analyses.

The SANDIA-BMINES finite element program uses the direct stiffness method of structural analysis. Displacement degrees of freedom are defined at nodal points located at the corners of the elements. Stress and strain values are, in general, computed at element centroids. Nodal point forces, which include external loads and internal resisting forces, are combined into a global loads vector while the element stiffnesses are consolidated into a structural or global stiffness matrix. Incremental displacements are obtained from the equilibrium equations using a form of Cholesky decomposition which involves triangularization of the global stiffness matrix, reduction of the loads vector, and back substitution of the

reduced load vector into the triangularized stiffness matrix. Interested readers should consult Ref. 4 for detailed discussions of the element and material properties libraries, the computer processing features (i.e., multibuffering techniques which allow efficient out-of-core processing) and for discussions of other user oriented features such as the automatic mesh generator and the bandwidth minimizer. Discussions of the thermal stress analysis capabilities are found in Ref. 8.

## III. MODELING

A schematic diagram of the model used for analysis of the canister movement is shown in Figure 1. Axisymmetric meshes have been used for both the viscous flow and thermoelastic computations. The salt region in both cases extended to a radius of 500 m and to horizons 750 m above and below the canister. The canister initially was centrally positioned in this region.

Boundary conditions for the region are also indicated on Figure 1 for both the viscous flow analyses and the thermal analyses. Kinematic constraints of zero radial velocity existed along the centerline and along the outer radial boundary while zero axial velocity was imposed on the lower horizon. The upper surface was assumed to have zero applied traction vectors. Initially, the salt and canister are motionless.

The thermal boundary conditions are also shown in Figure 1 for both the steady-state and transient analyses. In the transient analyses all boundaries were assumed to have zero heat flux. Throughout the transient analyses, very little temperature rise at the boundary was observed ($< 1$ K), indicating that these boundary conditions remained valid. In the steady-state analyses, the boundary conditions consisted of requiring that all outside boundaries remained at the initial salt temperature. The initial temperature was 313 K and is constant throughout the region.

The heat source was modeled with several point sources within the canister volume. These point sources decayed in the transient analyses with a 30 year half life. In the steady-state analyses the heat source was assumed to have a constant value equal to the maximum (initial) source strength for all times.

The finite element mesh used for both the heat transfer and creeping viscous flow computations is shown in Figure 2. The central portion of the mesh has been enlarged to show details of the mesh in the vicinity of the canister. The canister is represented by the two elements along the region axis of symmetry and centered at 750 m depth. The total mesh consists of 208 triangular elements. Each element has six nodal points giving a quadratic approximation for velocity and a linear pressure approximation. The radius (maximum) of the canister is 0.625 m at its center and has a double cone shape. The overall length is approximately 3 m. A second mesh was constructed for viscous flow computations in which finer discretization was imposed around the canister. This allowed for modeling a smaller radius (.278 m maximum at the center) canister. This mesh has 272 triangular elements, 603 velocity nodal points, and 437 pressure nodal points. Details of the zone near the canister are shown in Figure 3.

In the thermoelastic analyses the left hand (inner) boundary simulates the centerline of this axisymmetric model; only vertical motion was allowed along this axis. No radial motion was allowed along the outer boundary of the model but the nodal points along this surface were free to move vertically. The bottom boundary was assumed to be rigid, i.e., neither horizontal nor vertical motion was allowed. The top of the model had no displacement or traction boundary conditions imposed. The transient temperature fields computed using the COUPLEFLO program were used as input to the thermoelastic analysis.

The finite element mesh used in the thermoelastic model consists of 680 quadrilateral elements. Each element has four nodal points (one at each corner of the element) and two displacement degrees of freedom, u and

v, at each node. Bilinear displacement functions are used to represent the variation of the displacement components within an element. There are 735 nodal points in the mesh. After the boundary conditions have been applied, there are 1369 degrees of freedom remaining in the mesh. A portion of the mesh in the region nearest the canister is shown in Figure 4.

The material property values used in the analyses are the best estimates currently available. In the course of the analyses, several values of viscosity and conductivity were considered within the ranges of measured values. The property values are summarized in Table 1 with the sources of information.

## IV. RESULTS OF THE ANALYSES

Before analyzing canister movement associated with buoyant rising of the salt environment, a test case involving the sinking of a nonheat producing canister in an isothermal salt medium was examined. The predicted downward velocity was quite small, 29 pm/sec (24 m/1000 yr), for salt with a viscosity ($\mu$) equal to $0.5 \times 10^{14}$ Pa-sec. This velocity compares well with the velocity of 23 pm/sec (19.2 m/1000 yr) computed using a simple Stokes' sphere model in which the drag force was equivalent to that of a sphere with the same diameter as the canister approximation in the finite element solution.

Coupled transient analyses of the canister and salt motion were performed for models with constant and with variable salt viscosity. The salt conductivity in these analyses corresponds to the temperature dependent relationship listed in Table 2. Analysis using constant viscosity ($\mu = 0.5 \times 10^{15}$ Pa-sec) has been carried out to a time of 10 years. Initially, the canister began to sink since the surrounding salt was isothermal and the canister density (4100 kg/m$^3$) was greater than the salt. Heat from the wastes raised the salt temperature near the canister, providing the buoyant force necessary to start upward flow of the salt. The total canister velocity as a result of the upward salt velocity diminished. Eventually, the strength of the convective cell of the salt was sufficient to give the canister itself an upward velocity. The maximum canister velocity obtained during the 10 year period of analysis was 1.5 pm/sec. The total displacement during this time was .0001 m.

The transient analysis of the salt canister system using a model with temperature dependent salt viscosity (Table 1) has been performed using

COUPLEFLO for times out to approximately 150 years. Again the canister started from rest in an isothermal salt medium and began to sink. Using the temperature dependent viscosity model, however, the downward velocity of the canister initially increased as salt in the viscosity of the canister was heated. This was a result of the reduced viscosity of salt near the canister allowing the canister velocity relative to the salt to increase faster than the convective cell formed in the salt. Eventually, the convective cell gained strength and reduced the total canister velocity. After approximately 35 years the canister velocity became positive and subsequently obtained a peak upward velocity of 0.1 pm/sec. After approximately 125 years, the convective cell velocity had diminished and the canister began to move downward again. The total displacement during the 150 years of analysis was -.0003 m. The velocity history for the 150 year period is shown in Figure 5. The thermal history for points within the canister, at 10 m away from the canister, and 30 m away from the canister have been plotted in Figure 6. The convective circulation associated with the flow of salt can be readily seen from the velocity field depicted in Figure 7. Arrows in this figure indicate the direction of flow and are not proportional in length to the velocity magnitude.

Steady-state analyses were performed to provide an upper bound on the magnitude of canister velocities. In these analyses the canister heat output was assumed to be constant and to equal the maximum (initial) power of the wastes. A variety of cases have been examined to study the effects of different canister densities, variable and constant viscosity, variable and constant thermal conductivity, and canister mesh sizes. The results of these analyses are presented in Table 2. It is important to note that the velocities predicted in the steady-state analyses cannot be

used to predict movement beyond periods in which significant heating occurs. Rather, predicted velocities can only be interpreted as maximum upper bounds of velocity for some time during heating (less than 3000 years from time of emplacement).

The greatest upward velocity (26.5 pm/sec) was predicted for the case of constant viscosity and conductivity.(A) In this case the canister density was 4100 kg/m. The canister velocity decreases when temperature dependent conductivity was included in the model.(B) This was due to steeper thermal gradients near the canister that produced a smaller zone of low density salt. Thus, the driving force of the convective cell was less. By considering the temperature dependent viscosity of the salt, the canister's upward velocity was observed to diminish further.(E) This was because the reduced viscosity in the vicinity of the canister (hot zone) increased the canister's velocity relative to the salt more than it increased the velocity of the convective cell within the salt medium. The effect of varying the canister's density is shown in Figure 8. The density of 5800 kg/m can be seen to produce almost zero velocity.(F) In this case the canister was sinking in the salt with nearly the same velocity that the salt was rising. As the canister density decreased,(C)(D) the velocity of the canister in the salt decreased and the overall motion of the canister was upward.

The effect of meshing was also examined. The previous results were obtained using a relatively large canister radius ($r = .615$ m at the widest point). Specifying a smaller radius ($r = .276$ m) resulted in larger drag forces relative to the buoyant forces. (compare G w/ E) Thus, the upward velocity of the canister increased. For the constant salt viscosity ($\mu = .5 \times 10^{14}$ Pa-sec) and constant salt thermal conductivity the canister

velocity was 283 pm/sec[11]; whereas, for variable conductivity and viscosity (Table 1) the canister velocity was 2.5 pm/s.[6] In both cases the canister density was 4100 kg/m$^3$. The convective cell salt velocities and temperature distributions were the same for both mesh configurations.

The displacement of the surface at the repository centerline, as predicted by the thermoelastic model, is shown in Fig. 9. The maximum amount of surface motion which can result from the emplacement of the canister occurred at this point. The motion was once again quite small, i.e., less than .15 mm after 30 years. The canister rise due to expansion of the salt was at least an order of magnitude less than the surface motion.

It should be noted that in calculations (see Ref. 9) simulating the response of a large repository the surface motion increases with time for approximately the first 100 years and then remains relatively constant during the next several hundred years. It would, therefore, be unrealistic to extrapolate the results shown in Fig. 9 to long periods of time.

The results were also examined in terms of the validity of the assumption that inertia terms could be neglected from Equation (1). Equation (1), including inertia terms, can be written as follows:

$$\sigma_{ij,j} - \rho(\dot{u}_i - g_i) = 0 \ . \qquad (7)$$

In the analyses conducted, acceleration of the velocity field, $\dot{u}_i$, was small in comparison to the gravitational constant, $g_i$. Thus, the quantity $(\dot{u} - g_i)$ is closely approximated by $(-g_i)$. This indicates that neglecting inertia terms in valid.

## V. CONCLUSIONS

The analyses performed indicate that very little canister movement will result during the heat producing life of the waste canisters. The transient analyses show that initially the canister will sink. Due to the formation of a convective cell in the salt from heating by the wastes, the canister will rise. Eventually, as the convective cell diminishes the canister begins to sink again. Predicted displacements are less than a canister length during this process. The steady-state analyses provide upper bounds on the magnitudes of upward velocity possible during heating. In all cases, the velocities are sufficiently small to indicate very little movement will occur while the canister is capable of producing heat. The thermoelastic analyses predict little surface upheaval and indicate that the free expansion assumption used in the viscous flow analysis is reasonable.

The analyses performed apply only to a single canister in a large salt medium. The combined effect of many canisters cannot be inferred from superposition of the single canister results. Separate analyses are being performed to address the multiple canister problem.

## REFERENCES


1. Sato, A. and E. G. Thompson, "Finite Element Models for Creeping Convection," Journal of Computational Physics, 22, 1976.
2. Thompson, E. G., "Average and Complete Incompressibility in the Finite Element Method," International Journal for Numerical Methods in Engineering, Vol. 9, 925-932, 1975.
3. Dawson, P. R., "Finite Element Thermomechanical Models for Metal Forming," Ph.D. Thesis, Colorado State University, Fort Collins, CO, Fall, 1976.
4. Isenberg, Jeremy, "Analytical Modeling of Rock-Structure Interaction," 3 Volumes, Final Technical Report of ARPA Contract H0220035, Agbabian, Associates, El Segundo, CA, April 1973.
5. Personal communication with W. Wawersik, Division 5163, Sandia Laboratories, Albuquerque, NM.
6. Baumeister, Theodore, (Editor), Mark's Standard Handbook for Mechanical Engineers, Seventh Edition, McGraw-Hill Book Company, New York, 1967.
7. Thermomechanical Properties of Matter, Purdue University, Thermophysical Properties Research Center, 1970.
8. Tillerson, J. R. and M. M. Madsen, "Thermoelastic Capabilities of the SANDIA-BMINES Program," SAND-77-0378, Sandia Laboratories, Albuquerque, NM.
9. Dawson, P. R. and J. R. Tillerson, "Salt Motion Following Nuclear Waste Disposal," Proceedings of the International Conference on Evaluation and Prediction of Subsidence, Pensacola, FL, Jan. 15-20, 1977.

TABLE 1

Material Properties

| | | | | |
|---|---|---|---|---|
| **Salt:** | | | | |
| Density | 2167 $kg/m^3$ | | | TPRC [7] |
| Specific heat | 921 $\frac{watt\text{-}sec}{kg\ K}$ | | | TPRC [7] |
| Conductivity | 3 $\frac{watt}{m\ K}$ at 500 K | | | Memo from R. Acton to D. Powers of 4/20/76 |
| | 5 $\frac{watt}{m\ K}$ at 300 K | | | |
| Expansivity (Volumetric) | $1.2 \times 10^{-4}/K$ | | | |
| Viscosity - Variable | $0.455 \times 10^{4} e^{\frac{8589}{T}}$ | Pa-sec | $T < 383$ K | |
| | $0.25 \times 10^{14}$ | Pa-sec | $T > 383$ K | Personal communication with W. Wawersik - 5163 |
| Constant | $0.5 \times 10^{15}$ | Pa-sec | | |
| Bulk modulus | K = 13.1 GPa | | | Source - RE/SPEC Report RSI-0030, June 1975 |
| Shear modulus | G = 5.03 GPa | | | |
| **Canister*:** | | | | |
| Density | Varying between 2000 and 5800 $kg/m^3$ | | | |
| Specific heat | 500 $\frac{watt\text{-}sec}{kg\ K}$ | | | Mark's Handbook [6] |
| Conductivity | 200 $\frac{watt}{m\ K}$ | | | Mark's Handbook [6] |
| Expansivity | Neglected | | | |
| Viscosity | $1 \times 10^{20}$ Pa-sec (rigid) | | | |
| Heat generation rate (Initial) | 3.5 kw/canister | | | Personal communication with G. Barr - 1141 |

*Properties of steel used

TABLE 2

Steady-State Canister Movement†

| Case | Conductivity | Viscosity | Canister Density | Canister Centerline Radius | Velocity ($\times 10^{10}$ m/sec) | Maximum Distance Traveled in the First 3000 Years After Emplacement |
|---|---|---|---|---|---|---|
| A | Constant | Constant | 4100 | .625 | .265 | 2.51 m |
| B | Variable | Constant | 4100 | .625 | .215 | 2.03 |
| C | V | V | 2000 | .625 | .037 | 0.35 |
| D | V | V | 3000 | .625 | .027 | 0.26 |
| E | V | V | 4100 | .625 | .0165 | 0.16 |
| F | V | V | 5800 | .625 | -.0001 | -.001 |
| G | V | V | 4100 | .278 | .025 | .25 |
| H | C | C* | 4100 | .278 | 2.83 | 28.3 |
| I | V | C* | 4100 | .625 | 2.09 | 20.9 |

Conductivity — Constant: $4.0 \frac{\text{watt}}{\text{m K}}$

Variable: $10.76\, e^{-2.554 \times 10^{-3} T} \frac{\text{watt}}{\text{m K}}$

Viscosity — Constant: $\mu = 0.5 \times 10^{15}$ Pa-sec

Variable: $\mu = .455 \times 10^{4}\, e^{8589/T}$ Pa-sec for $T \geq 383$ K

$\mu = 0.25 \times 10^{14}$ Pa-sec for $T < 383$ K

*Viscosity $\mu = 0.5 \times 10^{14}$ Pa-sec (extremely low)

†Steady-state analyses provide only an upper bound to the maximum canister velocity. The results cannot be used to determine overall movement over long periods of time. Rather, velocities can only be used to place an upper bound on movement while movement is occurring (times less than 3000 years). During the first 3000 years following emplacement, the use of a constant source equal to the initial (maximum) power provides 70 times too much energy to the system.

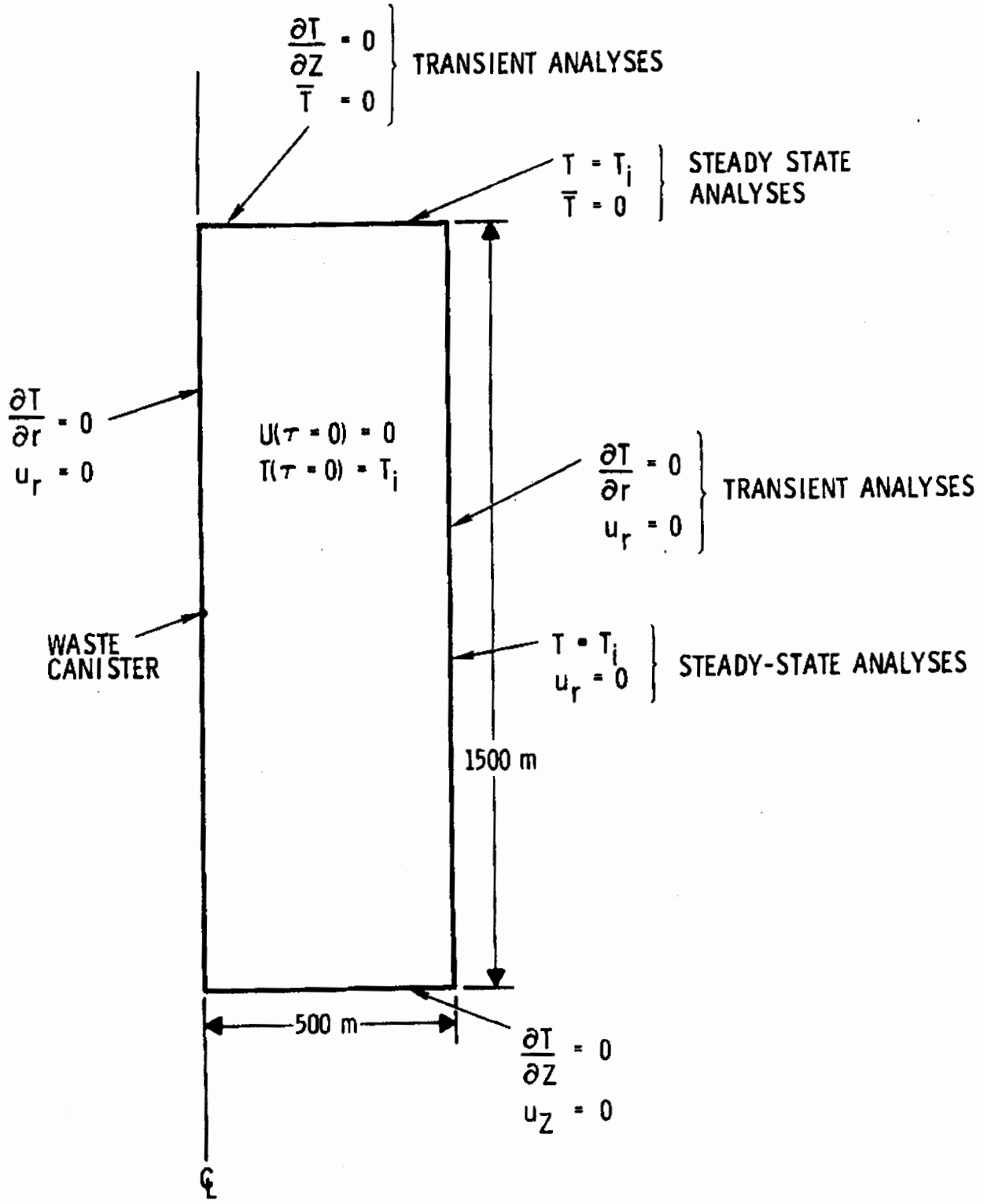


Figure 1. Canister Movement Axisymmetric Model

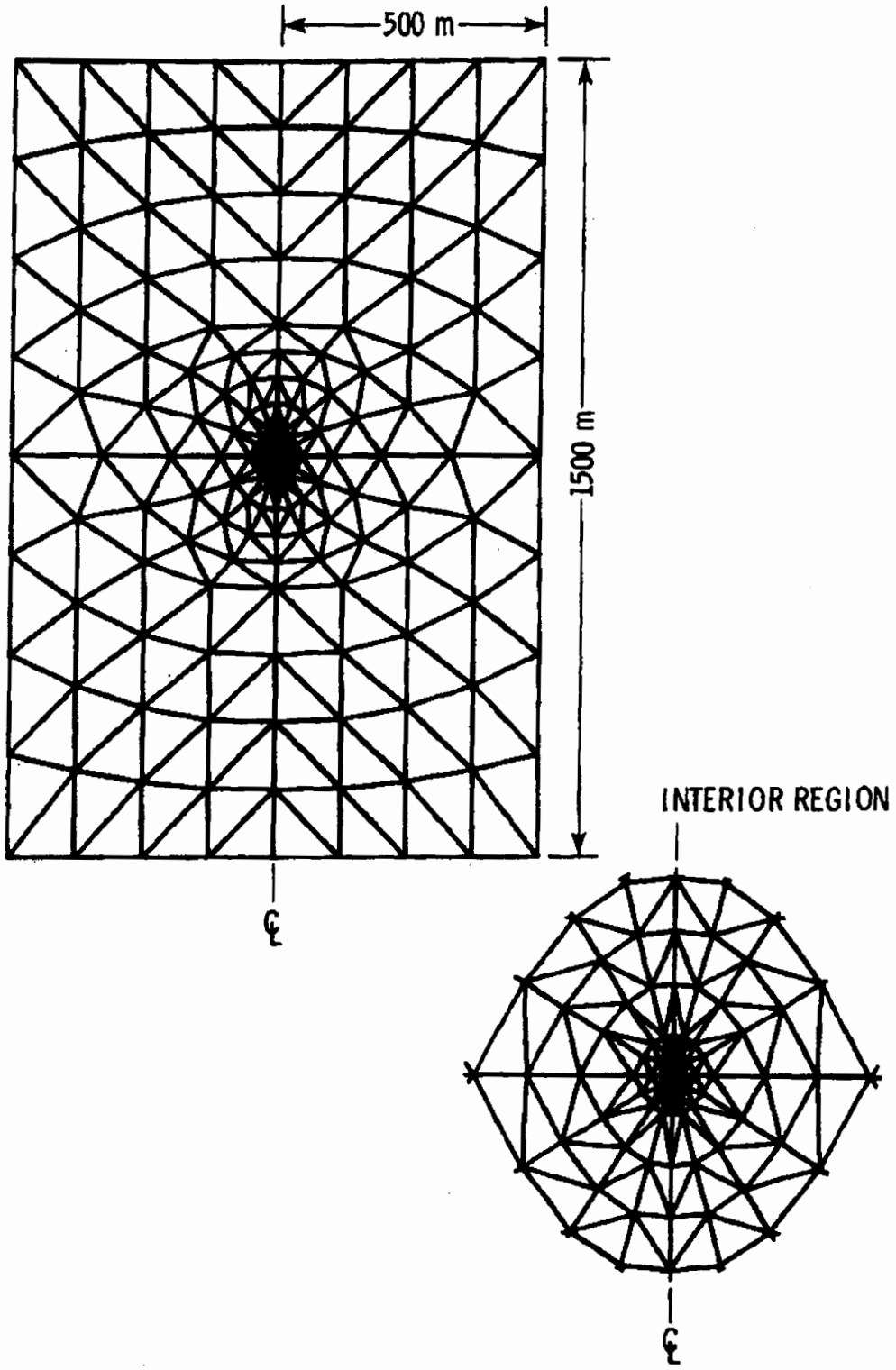


Figure 2. Viscoplastic Flow and Heat Transfer Coarse Mesh

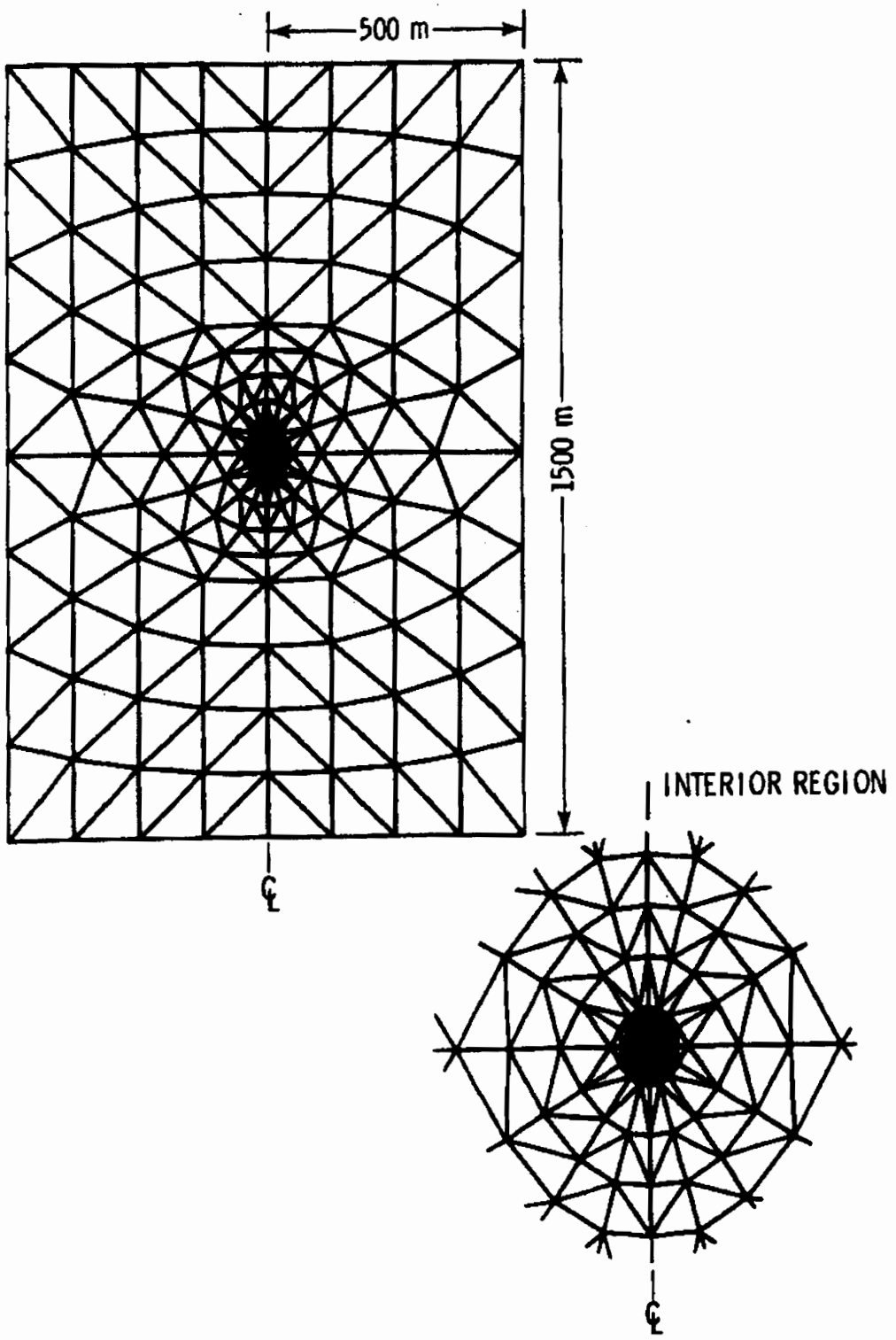


Figure 3. Viscoplastic Flow and Heat Transfer Fine Mesh

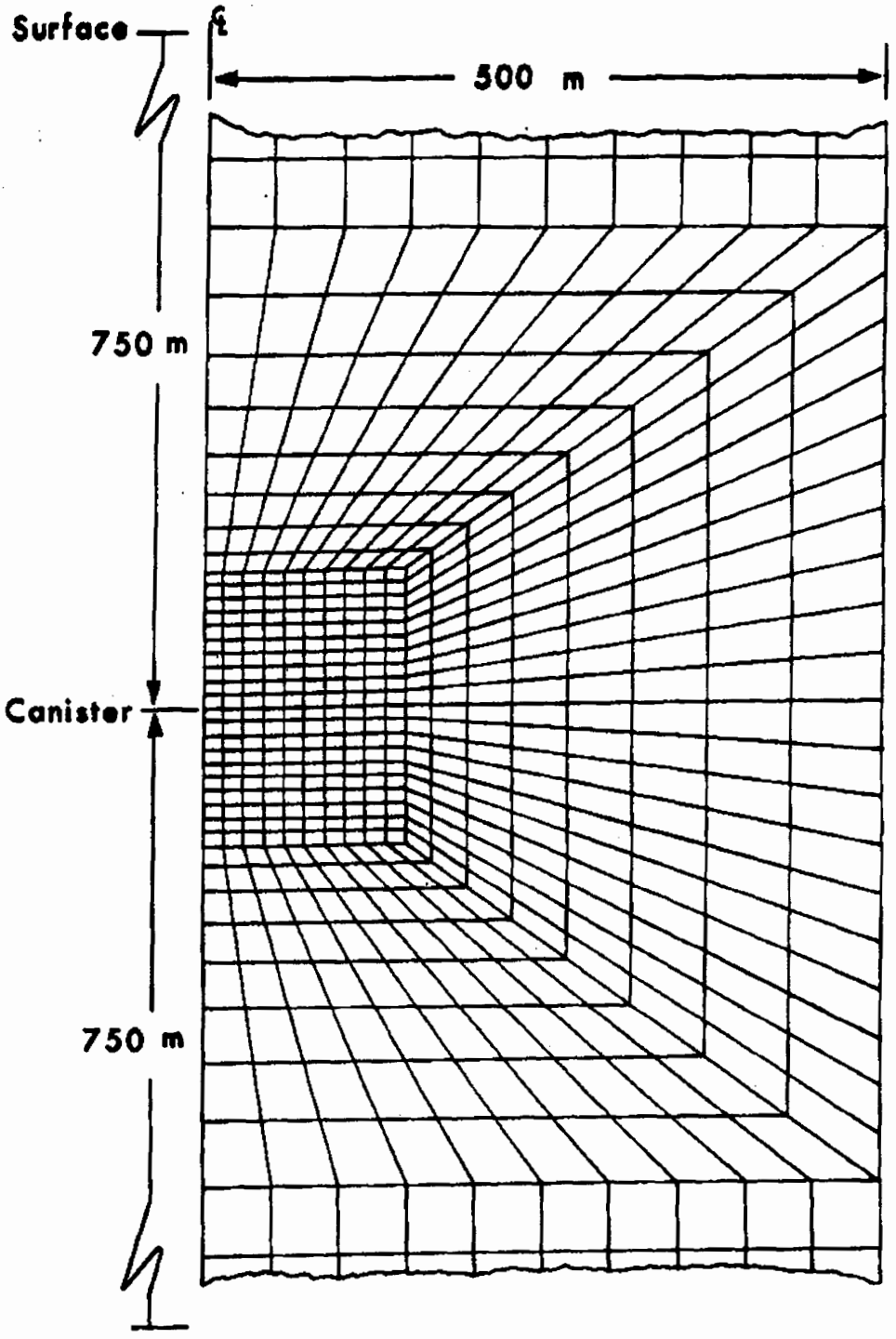


Figure 4. Thermoelastic Finite Element Mesh

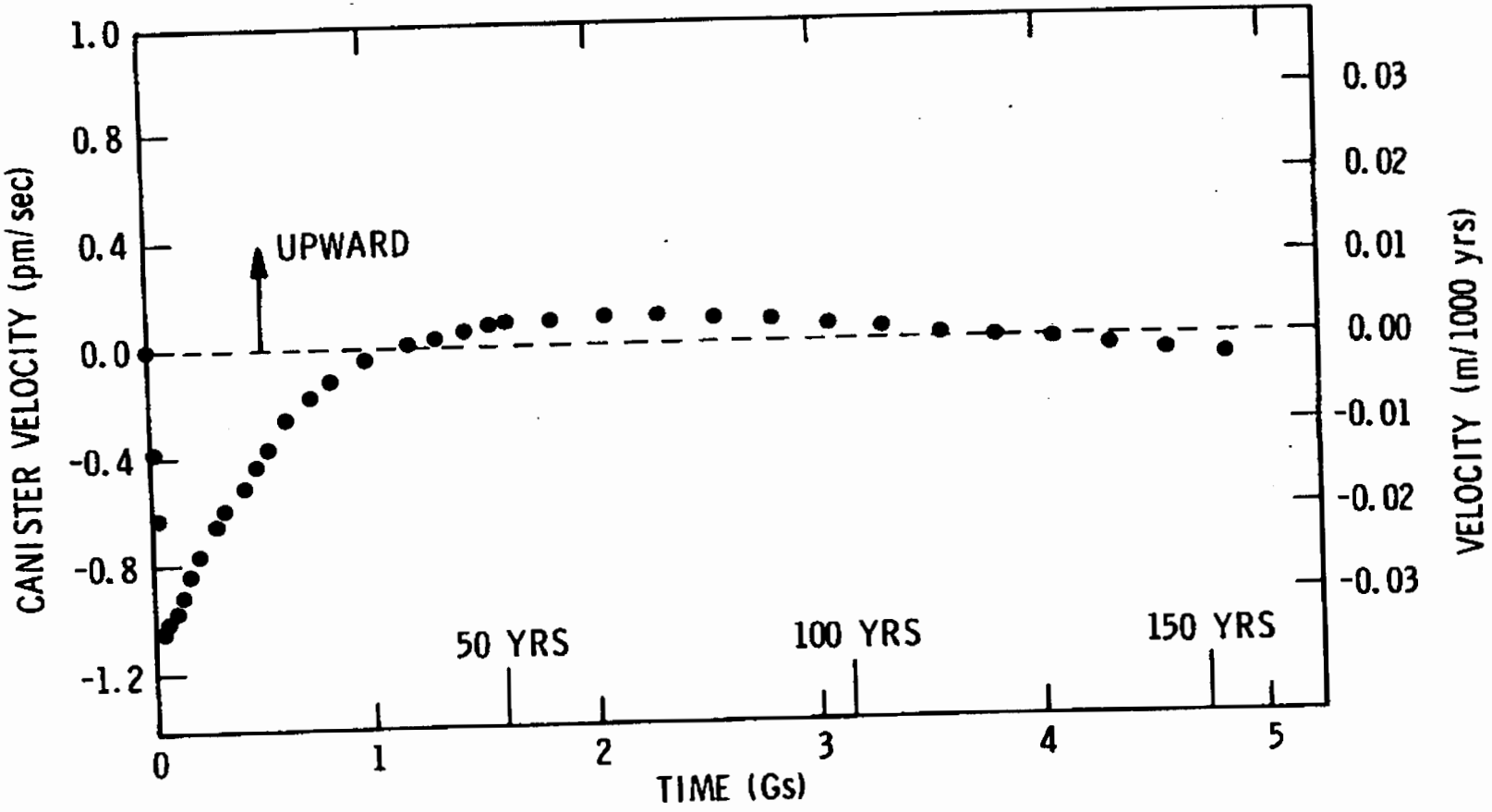


Figure 5. Canister Velocity History

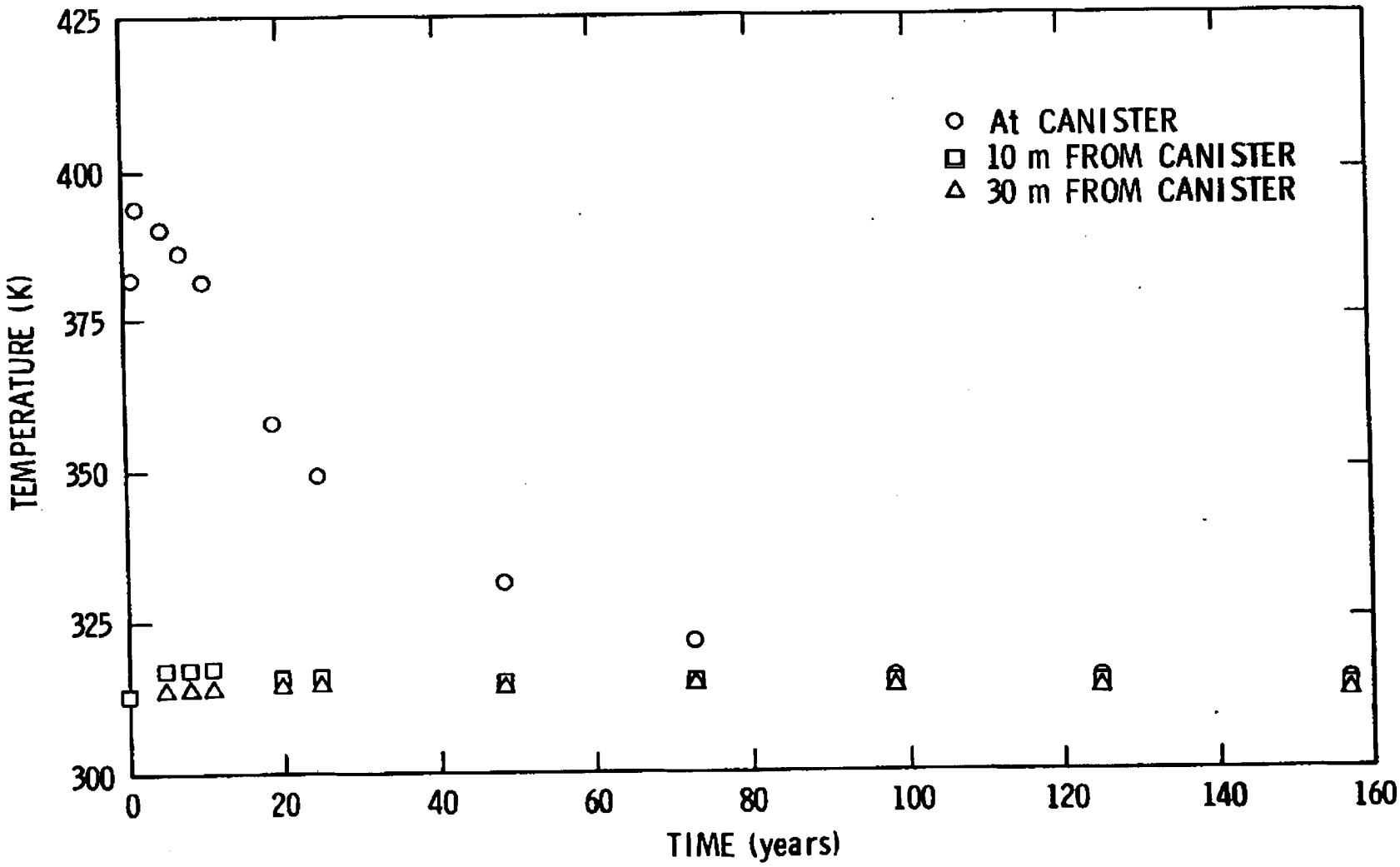


Figure 6. Salt Thermal History

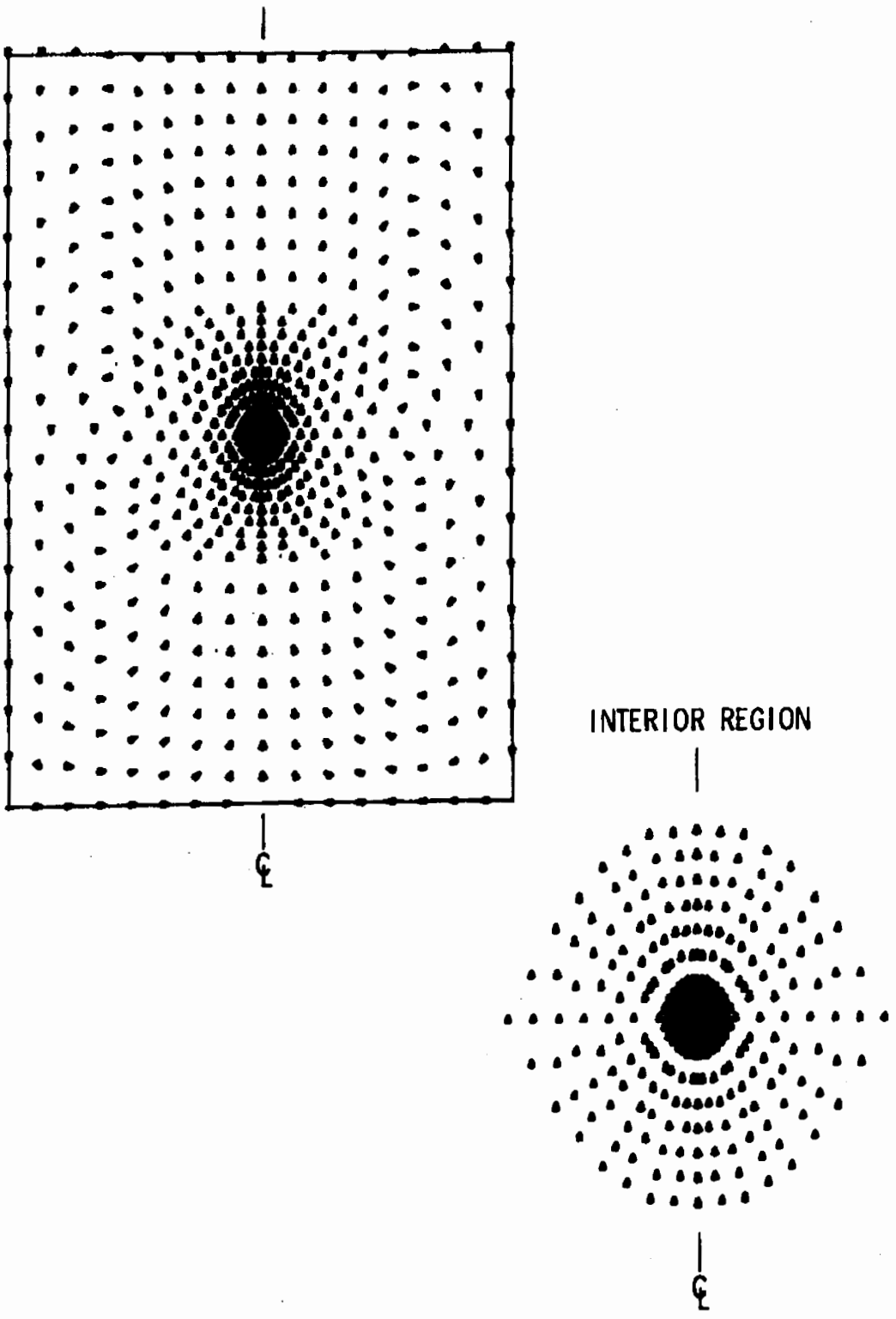


Figure 7. Salt Velocity Field

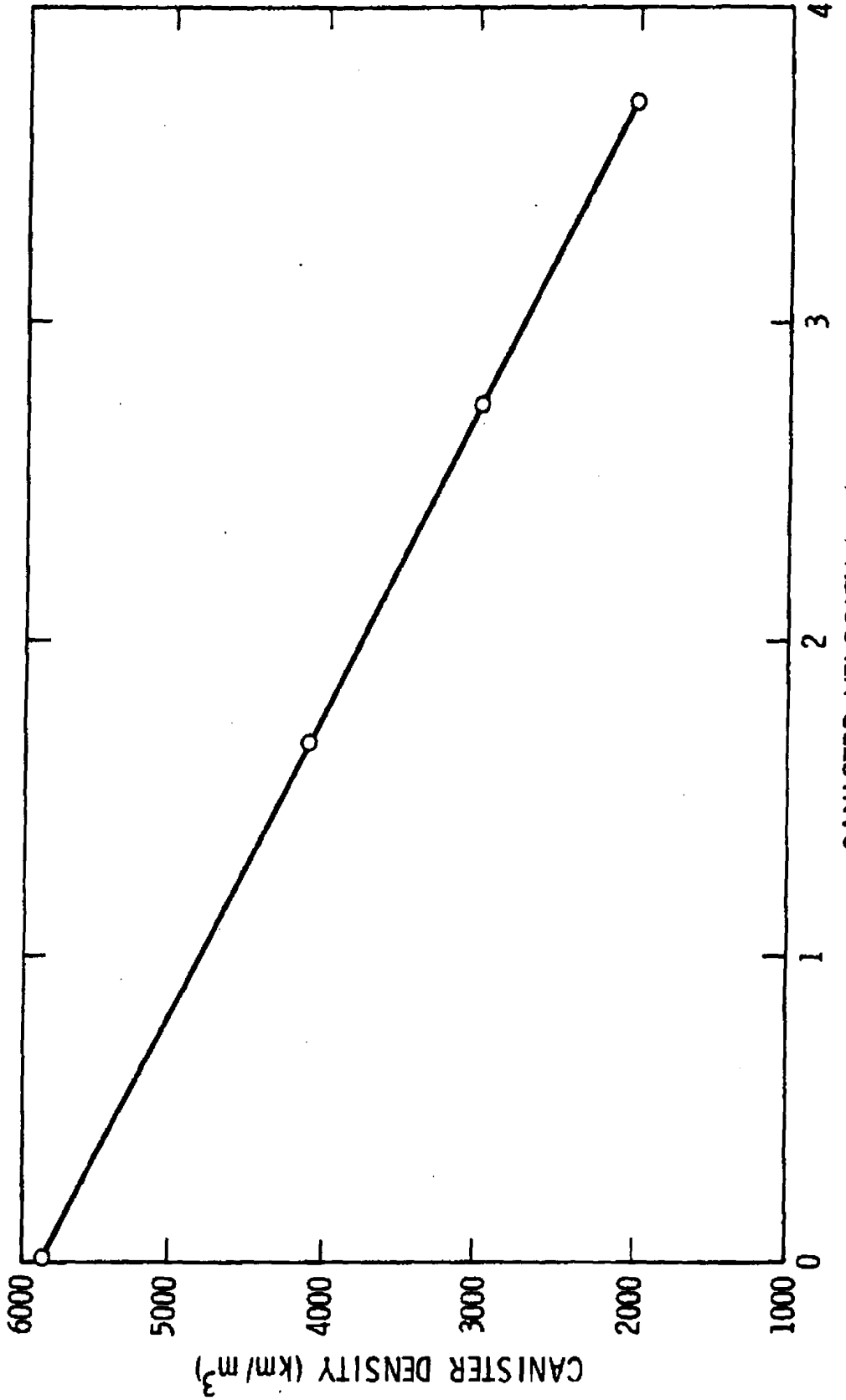


Figure 8. Canister Density Effect on Canister Velocity

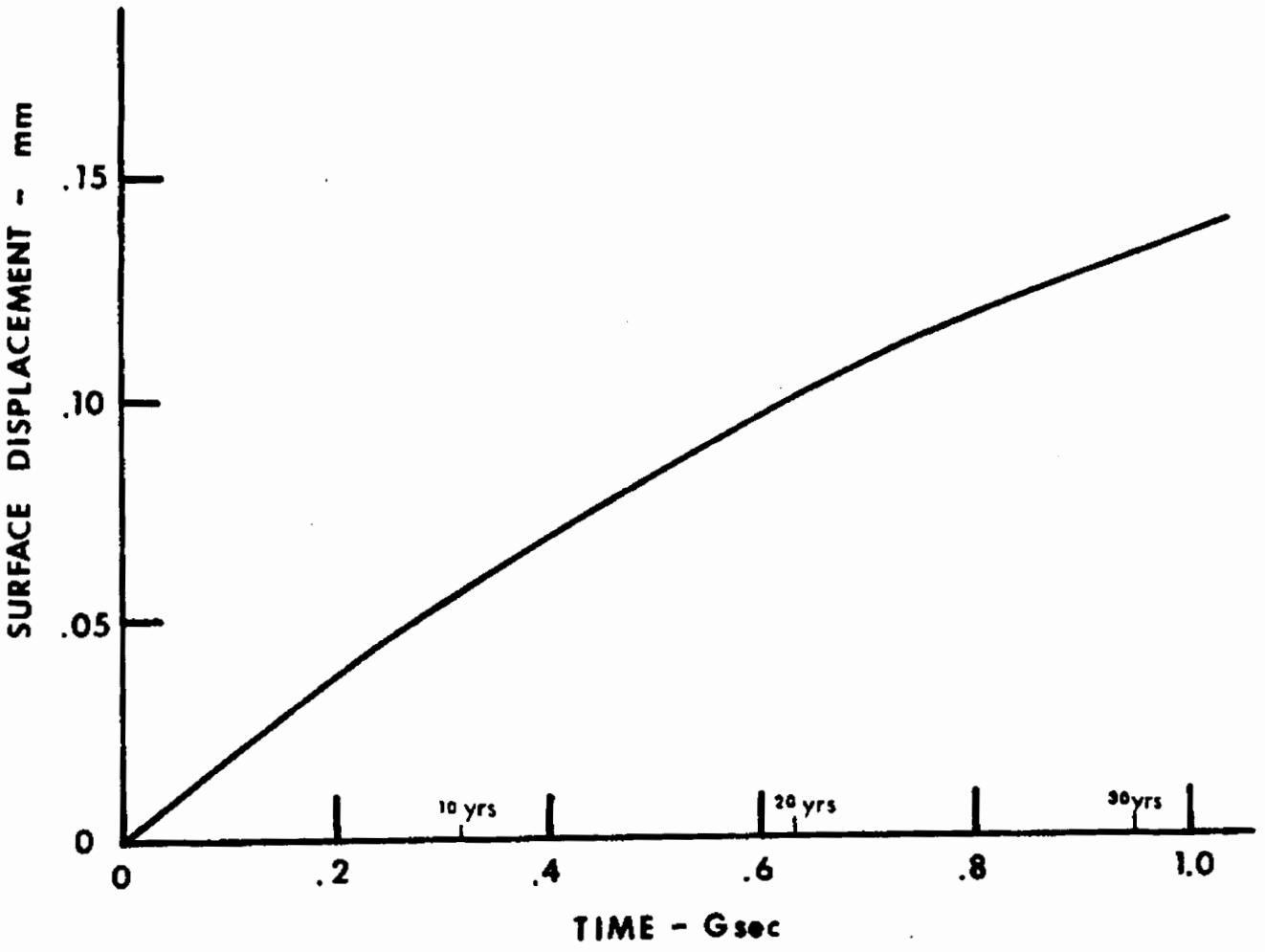


Figure 9. Surface Rise Resulting from Thermoelastic Behavior

UNLIMITED RELEASE

DISTRIBUTION:

W. P. Armstrong
U. S. Department of Energy
Albuquerque Operations Office
P. O. Box 5400
Albuquerque, NM 87185

Dr. D. L. Vieth
U. S. Department of Energy
Headquarters
Washington, D. C. 20545
ATTN: R. Ng

Dr. W. C. McClain
Union Carbide Corporation
Office of Waste Isolation
P. O. Box Y, Bldg. 9102-2
Oak Ridge, TN 37830

Dr. J. E. Russel
Union Carbide Corporation
Office of Waste Isolation
P. O. Box Y, Bldg. 9102-2
Oak Ridge, TN 37830

Dr. Paul Gnirk
RE/SPEC, Inc.
P. O. Box 725
Rapid City, SD 57701

Dr. Harry L. Browne, Manager
Business Development Nuclear Fuel Programs
Bechtel Inc.
P. O. Box 3965
San Francisco, CA 94119

Dr. Marvin H. Wilkening
New Mexico Institute of Mining and Technology
Socorro, NM 87801

University of California (3)
Los Alamos Scientific Laboratory
Los Alamos, NM 87545
ATTN: Dr. R. J. Bridwell MS 665
Dr. Charles Anderson MS 576
Dr. Phil Halleck MS 968

Dr. Paul Lykaudis
School of Nuclear Engineering
Purdue University
W. Lafayette, IN 47907

Dr. Alan Chockie
4800 Oak Grove Drive
Jet Propulsion Lab
Pasadena, CA

Prof. Gerald Schubert
Dept. of Earth & Space Science
UCLA
Los Angeles, CA 90024

Dr. Pete Borgo
BDM Corporation
2600 Yale Bldv., S. E.
Albuquerque, NM 87106

Dr. J. L. del Val
Electra De Viesgo, S.A.
Departmento Nuclear
Medio, 12-SANTANDER
SPAIN

Ken E. Davis
Subsurface Inc.
555 S. West Loop South
Suite 646
Bellaire, TX 77401

Dr. Peter Montegue
Southwest Research & Information Center
P. O. Box 4524
Albuquerque, NM 87106

Dr. Dave Bernstein
Science Application Inc.
8201 Capwell Drive
Oakland, CA 94621

Wayne E. Fisher (2)
Albuquerque Operations Office
U. S. Department of Energy
Class & Tech. Info. Division
P. O. Box 5400
Albuquerque, NM 87185

DISTRIBUTION (Cont'd):

Dr. J. Geertsma
Advisor to Management
KSEPL
6 Volmorlaan
Ryswgk, Netherlands

1111 J. F. Cuderman
5100 J. K. Galt
ATTN: 5110 F. L. Vook
5120 G. J. Simmons
5130 G. A. Samara
5150 J. E. Schirber
5160 W. Herrmann
ATTN: 5166 A. J. Chabai
5167 B. M. Butcher
5162 L. D. Bertholf
5162 P. F. Chavez
5162 P. R. Dawson (20)
5162 R. J. Lawrence
5162 M. M. Madsen
5162 J. R. Tillerson (20)
5163 D. E. Munson
5163 J. B. Rundle
5163 H. J. Sutherland
5163 W. Wawersik
5300 O. E. Jones
5310 W. D. Weart
5311 L. R. Hill
5311 G. E. Barr
5311 D. W. Powers
5311 M. A. Molecke
5311 A. R. Sattler
5311 R. E. Wayland
5314 M. L. Merritt
ATTN: F. W. Bingham
5330 R. W. Lynch
5336 D. R. Anderson
5336 R. D. Klett
5336 D. M. Talbert
5337 J. L. Krumhansl
5337 A. R. Lappin
5337 R. C. Lincoln
5340 M. L. Kramm
5341 L. W. Scully
5341 P. D. O'Brien
5341 H. C. Shefelbine
5341 R. E. Stinebaugh
5341 W. E. Wowak
5342 J. W. McKiernan
ATTN: H. C. Walker
8266 Tech. Library
3141 Tech. Library (5)
3151 Tech. Writing (3)
For DOE/TIC (Unlimited Release)
DOE/TIC (25)
(R. P. Campbell 3172-3)